An Improved Approach for Evapotranspiration Estimation Using Water Balance Equation: Case Study of Yangtze River Basin

Qiong Li [1,*], Zhicai Luo [1], Bo Zhong [2,3] and Hao Zhou [1,*]

[1]   MOE Key Laboratory of Fundamental Physical Quantities Measurement, Hubei Key Laboratory of Gravitation and Quantum Physics, School of Physics, Huazhong University of Science and Technology, Wuhan 430074, China; zcluo@hust.edu.cn
[2]   School of Geodesy and Geomatics, Wuhan University, Wuhan 430079, China; bozhong@sgg.whu.edu.cn
[3]   Key Laboratory of Geospace Environment and Geodesy, Ministry of Education, Wuhan University, Wuhan 430079, China
[*]   Correspondence: qiongli@hust.edu.cn (Q.L.); zhouh@hust.edu.cn (H.Z.); Tel.: +86-134-7612-1382 (Q.L.); +86-155-2781-4858 (H.Z.)

check for updates

Abstract: Evapotranspiration (ET) is a critical component of the water cycle, and it plays an important role in global water exchange and energy flow. However, accurate estimation and numerical simulation of regional ET remain difficult. In this work, based on the water balance equation, an improved regional ET estimating approach was developed by using Gravity Recovery and Climate Experiment (GRACE), daily precipitation, and discharge data. Firstly, the method and algorithm were validated by simulation study. Compared with ET estimated from previous methods, the result derived from our method present significant improvement, with the correlation coefficient great than 0.9. Secondly, using our improved method, the spatially averaged ET over the Yangtze River Basin (YRB) was computed for the period 2003–2013. The ET estimations were in good consistency with different ET products, and the mean annual value of ET estimation over the YRB was close to the difference between precipitation and discharge over the YRB. Thirdly, the comparison between ET estimation and independent estimates of meteorological factors and soil moisture over the entire YRB were conducted through the entire YRB. The analysis indicated that near-surface temperature, as responsive to atmospheric demand, was the limiting factor of time variation of ET, with the correlation coefficients of 0.69. We also analyzed the relationship between the mean annual ET and atmospheric demand for seven subcatchments of the YRB, which indicated that the spatial distribution characteristics of ET estimated by our method were in accord with atmospheric conditions. These results indicated the good performance of our improved approach in estimating ET variations over the YRB. It also demonstrates the applicability of GRACE to the analysis of hydrological features such as regional ET.

Keywords: evapotranspiration; GRACE; Yangtze River Basin; water balance equation

1. Introduction

Evapotranspiration (ET) plays an important role in global water exchange and energy flow across the hydrosphere, atmosphere, and biosphere [1,2]. Accurate quantification of ET is elementary for understanding ET and its response relationship with global or regional environmental changes, as well as for planning and designing water supply systems and sustainable use of water resources [3,4]. Currently, estimations of ET are based mostly on observations from ground-based hydrological stations and satellite remote sensing, or they are simulated using a land surface model (LSM). Ground-based

meteorological observation of ET by lysimeter is one of the most accurate estimation techniques; however, the sparsity of the network of observing stations limits the understanding of ET on the global scale, and even on the scale of some large basins. Satellite remote sensing can overcome some of the limitations of ground-based observations, and it provides a method with which to investigate the regional to global spatiotemporal variability of ET. Based on regional evaporation estimates from flux towers and remote sensing data acquired by the Moderate Resolution Imaging Spectroradiometer (MODIS), Mu et al. [5] used Penman–Monteith equations to estimate the global spatiotemporal variability of ET, considering both the surface energy partitioning process and the environmental constraints on ET. Fisher et al. [6] estimated actual global ET over a 1° grid based on modified Priestley–Taylor equations using Advanced Very High Resolution Radiometer data. The Global Land Data Assimilation System (GLDAS) [7] constrains the modeled land surface states by using the ground- and space-based observation system, and provides near-real-time information of hydro-meteorological data of the earth's surface. Moreover, it also provides ET estimations for four different land surface models (LSMs): Mosaic, the variable infiltration capacity (VIC) model, the community land model (CLM), and Noah. Compared with ground-based observations, satellite-derived ET and GLDAS estimations of ET have advantages in terms of their global coverage, higher spatial resolution, and reasonable assessment of the spatial variation of ET. However, satellite remote sensing retrievals of ET and ET estimations based on LSMs are highly dependent on climate, vegetation structure, and precipitation intensity, while complex land conditions limit the applicability in certain regions. For instance, most land surface and atmospheric models do not consider irrigation, which with all else being equal, would lead to a low bias in ET when averaged over large scales.

Spatially averaged ET on the basin or the continental scale can be estimated using the water balance equation: $ET = P - R - \Delta S$. This calculates ET as the residual between precipitation (P) and the sum of river discharge (R) and terrestrial water storage change (TWSC as well as ΔS) from GRACE satellite-based measurements [8–12]. Estimations of ET from GRACE satellite observations based on the water balance equation do not suffer the deficiency of ET from MODIS and GLDAS models. This is because the terrestrial water storage (TWS) from GRACE directly observes all the influencing factors, including human activities such as agriculture, irrigation, and impoundment by reservoirs [13–15]. The GRACE satellite has been measuring gravity changes on earth with unprecedented accuracy for over 15 years, since it was launched in March 2002. The capability of GRACE for monitoring earth's surface mass redistribution due to global or large-scale water storage changes has been documented by previous studies [16,17]. In recent years, the GRACE temporal gravity field models have been applied to the present-day mass redistribution within the earth system [18], covering global and local hydrological cycles [19,20], glacial mass variations [21,22], global sea level change [23,24] (Cazenave et al. 2009, Chen et al. 2005), and coseismic deformation [25–27]. Initially, research on TWS variations focused primarily on the level of agreement between hydrological models and GRACE-derived results, or on the detection of TWS anomalies caused by extreme climatic events [28–30] or human activity [31–33]. The long-term GRACE dataset has allowed recent applications of GRACE-derived water storage variations to consider estimations of important components of the hydrological cycle, such as ET [10,11,14] and river discharge, to calibrate hydrological models [34,35], or to improve LSMs [36,37].

Many studies that have estimated ET inferred from GRACE TWSC have used the method of Ramillien et al. [10] (Equation (5)), i.e., the TWSC is obtained from the monthly GRACE-derived TWS of the months before and after the given month. However, these TWSC cannot characterize the information for the given month, especially when the TWSC of the neighboring months are significantly different to each other. Rodell et al. [2] provided an equation that considers the difference in mean monthly total TWS between two consecutive months and daily P, R, and ET values to calculate the average monthly total ET in the two months denoted by the mean daily ET rates. This partially overcomes the disadvantages of the TWSC obtained using the method of Ramillien et al. [10]. However, the average monthly total ET in the two months is the running mean accumulation value, which is not normally used in hydrology. Therefore, we derived an improved method to calculate the monthly

mean ET by establishing relations between the monthly mean ET and daily precipitation, discharge, and GRACE-derived TWS based on the water balance equation.

The primary objective of this study was to verify the feasibility of the improved method and to examine ET estimations over the Yangtze River Basin (YRB) as a case study. We verified the efficacy of our method by comparing the monthly ET estimations from our method with those obtained from previous methods by simulation. Spatially averaged ET estimations over the YRB and its seven subcatchments were also calculated by combining GRACE monthly gravity field models and daily precipitation and discharge observations. The ET based on the water balance equation was compared with the GLDAS LSM-based ET, ET from MODIS, and ground-based observations to explore the characteristics of the differences for the YRB and each major subcatchment. The ET and TWS anomalies were also obtained to establish how ET influences TWS, especially in the extreme climatic conditions of drought that occurred in the YRB. We investigated the meteorological factors and soil moisture variations in the same period, which allowed us to identify the major hydroclimatic factor limiting ET variation over the YRB.

2. Study Area

The YRB lies within 24°–36° N, 90°–123° E, covering an area of 1.8×10^6 km^2 (Figure 1). The YRB exhibits a variety of topography, which can be characterized as descending in three stages from high in the west (5000 m at the river source on the Tibetan Plateau) to low in the east (below 500 m on the Yangtze River Delta Plain), as shown in Figure 1b. Although the total drainage area of the YRB is 1.8×10^6 km^2, the final gauging station on the river at Datong commands an area of only 1.7×10^6 km^2 because it is located at the upstream limit of tidal influence [38]. In this study, we subdivided the entire YRB catchment into 11 subcatchments (the boundaries of the YRB and of the subcatchments were provided by the Lake-Watershed Science Data Center of National Earth System Science Data Sharing Infrastructure (http://lake.geodata.cn). We focused on the seven subcatchments above the Datong station, shown in Figure 1a, as well as on the corresponding gauging stations for each subcatchment. The areas and the means of hydrological variables for each subcatchment and the entire basin for the period 2003–2013 are listed in Table 1. These statistical data of mean annual precipitation and temperature were recorded at 722 hydrographical and meteorological stations in China, and they were provided by the Climatic Data Center (http://data.cma.gov.cn) of the National Meteorological Information Center. The statistical results demonstrate that the area of the source of the river with the highest elevation has the least precipitation and the lowest temperature. Both the mean annual precipitation and the temperature increase across the catchment from northwest to southeast, reflect the monsoonal climate. Mean annual precipitation ranges from 720 mm in the Jinshajiang catchment to 1507 mm in the Poyang Lake catchment, and 85% of the annual precipitation occurs during April–October in the middle and lower reaches. The difference in mean annual temperature between the upstream and the downstream areas is very large, i.e., lowest (9.6 °C) in the Jinshajiang basin and highest (18.1 °C) in the Poyang Lake catchment, respectively.

Table 1. Mean annual precipitation (MAP) and mean annual temperature (MAT) for the period 2003–2013, watershed area, and gauging stations over each subcatchment.

Catchment	Station	Area (10^4 km^2)	MAP (mm)	MAT (°C)
Jinshajiang	Pingshan	45.86	720	9.6
Wujiang	Wulong	8.30	1029	15.3
Minjiang	Gaochang	13.54	948	11.8
Jialingjiang	Beibei	15.67	927	16.7
Hanjiang	Xiantao	14.47	918	15.9
Dongting Lake	Chenglingji	27.46	1261	17.0
Poyang Lake	Hukou	16.22	1507	18.1
Entire basin (YRB)	Datong	170.54	1059	14.4
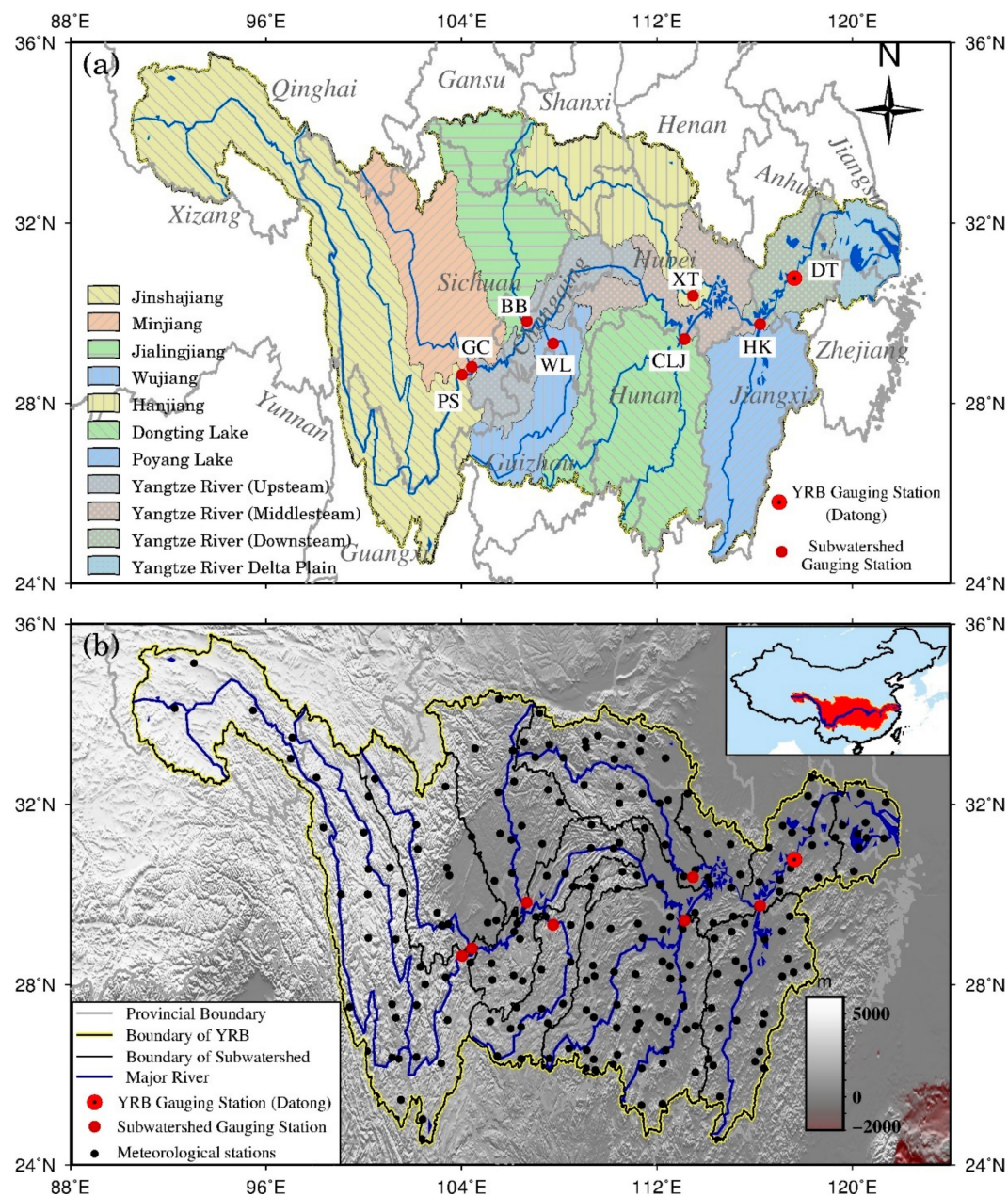
Figure 1. (**a**) Boundaries of the Yangtze River Basin (YRB) and its 11 subwatersheds, and (**b**) YRB topography and the locations of in situ measurements.

The widely varying climate and complex topography of the YRB makes it a promising test bed for the evaluation of water cycle systems under different climatic and land cover conditions. Although ET is an indispensable element of TWS, it remains the least well-understood component of the water balance equation because of its complex response mechanism. In particular, owing to the complex climatic conditions and fragile ecological environment of the YRB, it was difficult to model actual ET for this region. Though existing ET products have revealed certain features on the large scale and few ground-based meteorological stations observed actual ET in situ [39], it remains inadequate to display the temporal and long-term variations for each subcatchment. Therefore, this study was conducted using ground-based and satellite-derived data for the estimation of ET in the YRB, in order to analyze the interactions between ET and other hydrometeorological components.

3. Data and Methods

3.1. GRACE Data and TWSC

Here, the GRACE-derived TWS data were extracted to estimate ET over the YRB. Overall, 126 monthly average gravity field models from April 2002 to December 2013 were used in the study, which were provided by Release05 solutions from the Center for Space Research, University of Texas at Austin. Each monthly gravity field model consisted of fully normalized spherical harmonic coefficients up to degree and order 96. Here, $1° \times 1°$ gridded TWSs over the YRB were estimated from the GRACE monthly gravity field models using the 300 km Fan filter [40] and the P3M6 decorrelated filter [41], and the C20 series from GRACE were substituted by the time series of C20 from satellite laser ranging [42]. The $1° \times 1°$ gridded monthly terrestrial water storage anomalies (TWSA) were obtained from each monthly TWS minus the mean TWS of the entire period. As GRACE monthly gravity models are often nonconsecutive, missing monthly data were interpolated from time series solutions. The TWSC was considered as the variation during a specific period. When estimating ET using the method of Ramillien et al. [10], the TWSC for the *i*th month is

$$TWSC(i) = \frac{TWSA(i+1) - TWSA(i-1)}{2}. \tag{1}$$

when estimating ET using our method, the value of ΔS is the TWSC derived from GRACE in two consecutive months, which can be written as

$$\Delta S_{i,i+1} = TWSA(i+1) - TWSA(i). \tag{2}$$

3.2. Precipitation, Discharge, and ET

Here, the Global Precipitation Climatology Project (GPCP) One-Degree Daily (1DD) product (Version 1.2) was used to obtain the precipitation averaged over the YRB and the seven subcatchments. The GPCP product provides daily precipitation on a $1°$ grid over the entire globe for the period from October 1996 to the present. It is a merged analysis that incorporates precipitation estimates from both microwave-based data from the Special Sensor Microwave Imager and geosynchronous-orbit satellite infrared data, and quality-controlled surface rain gauge observations [43]. The other daily precipitation data used were China Ground Climate daily observation Data (CGCD) (Version 3.0) (http://data.cma.cn). There are 224 meteorological stations distributed throughout the YRB that have been operational between 1951 and the present (Figure 1b). Moreover, these meteorological stations were heterogeneously distributed over the YRB, and they were especially sparsely distributed in the northwest of YRB. Here, the daily average precipitation over the entire YRB and the seven subcatchments was estimated using a robust spatial averaging method. The monthly precipitation data of the two different products have high correlation (0.95 for the entire YRB); therefore, only the GPCP 1DD daily product was used to estimate ET in this study.

The discharge data used in this study were provided by the Changjiang Water Resources Commission of the Ministry of Water Resources. There are eight gauging stations on the upper and middle reaches of the Yangtze River (Figure 1, Table 1). The discharge data comprised daily observations from 2003 to 2013. We compared the mean annual values of *P* from the GPCP and *R* from in situ observations over the YRB with statistical observations from Changjiang and the Southwest River Water Resources Bulletin (CSWRB) (http://www.cjw.gov.cn) for the period 2003–2013. The mean annual values of *P* and *R* obtained from the data used in this study were 1059.2 mm/year and 465.9 mm/year, respectively, while the mean annual values of *P* and *R* obtained from the CSWRB were 1044.79 mm/year and 478.75 mm/year, respectively, i.e., the values were reasonably consistent.

Three different ET products (i.e., monthly ET products from GLDAS and MODIS and daily ET products from the CGCD) were used to evaluate the GRACE-based ET in this study. The GLDAS integrates satellite data and LSM data to generate a global distribution of land surface states

(e.g., ET). The ET outputs used were derived from four LSMs [7]: Mosaic, Noah, CLM, and VIC. The MODIS-derived estimates of ET were based on the Penman–Monteith method by combining remote sensing data and meteorological observations [5]. The monthly ET of the entire YRB and seven subcatchments were provided by the GLDAS and MODIS ET products without post-processing. The CGCD (Version 3.0) provided the daily average ET of the YRB region based on the data from the 224 meteorological stations, which observed daily ET by E-601B evaporator and small-sized evaporator. Daily ET estimates for the entire YRB and the seven subcatchments were obtained using the same spatial averaging method used for precipitation.

3.3. An Improved Approach for Estimation of Monthly ET

The hydrological water balance equation at the basin scale can be expressed as

$$\Delta S = P - R - ET, \tag{3}$$

where P is total precipitation, R is stream flow, ET is regional evapotranspiration over the watershed area, and ΔS is the TWSC for a specific time period.

The daily basin-scale water balance can be written as

$$\Delta S_{N_1,i} = P_{N_1,i} - R_{N_1,i} - ET_{N_1,i}, \tag{4}$$

where $P_{N_1,i}$, $R_{N_1,i}$, and $ET_{N_1,i}$ are the daily measurements of the ith day for N_1th month. Assuming that water storage for the beginning of the N_1th month is $S_0^{N_1}$, the water storage for the first day of the N_1th month could be written as

$$S_{N_1,1} = S_0^{N_1} + \Delta S_{N_1,1} = S_0^{N_1} + \left(P_{N_1,1} - R_{N_1,1} - ET_{N_1,1} \right). \tag{5}$$

The water storage for the ith day of the N_1th month could be written as

$$S_{N_1,i} = S_0^{N_1} + \sum_{N_1,n=1}^{N_1,i} \Delta S_{N_1,n}. \tag{6}$$

Rewriting Equation (6) for all days D_1 in the N_1th month and summing yields:

$$S_{N_1,1} + S_{N_1,2} + \cdots + S_{N_1,D_1} = S_0^{N_1} + \sum_{N_1,i=1}^{N_1,1} \Delta S_{N_1,i} + S_0^{N_1} + \sum_{N_1,i=1}^{N_1,2} \Delta S_{N_1,i} + \cdots + S_0^{N_1} + \sum_{N_1,i=1}^{N_1,D_1} \Delta S_{N_1,i} = D_1 \cdot S_0^{N_1} + \sum_{N_1,i=1}^{N_1,D_1} \sum_{j=1}^{i} \Delta S_{N_1,j}. \tag{7}$$

Then, the average water storage for the N_1th month can be written as

$$\overline{S}_{N_1} = S_0^{N_1} + \frac{1}{D_1} \sum_{N_1,i=1}^{N_1,D_1} \sum_{j=1}^{i} \Delta S_{N_1,j} = S_0^{N_1} + \frac{1}{D_1} \sum_{N_1,i=1}^{N_1,D_1} (D_1 + 1 - i) \Delta S_{N_1,i}. \tag{8}$$

The second term on the right-hand side of Equation (8) is the running mean accumulation of water storage (or hydrological elements), which is not normally used in hydrology [2]. However, the term $\overline{S}_{N_1}$ closely approximates the water storage observed by the GRACE satellite. Similarly, the average water storage for the N_2th month is

$$\overline{S}_{N_2} = S_0^{N_2} + \frac{1}{D_2} \sum_{N_2,i=1}^{N_2,D_2} \sum_{j=1}^{i} \Delta S_{N_2,j} = S_0^{N_2} + \frac{1}{D_2} \sum_{N_2,i=1}^{N_2,D_2} (D_2 + 1 - i) \Delta S_{N_2,i}. \tag{9}$$

If $N_2 = N_1 + 1$, the relationship between $S_0^{N_1}$ and $S_0^{N_2}$ is

$$S_0^{N_2} = S_0^{N_1} + \sum_{N_1,i=1}^{N_1,D_1} \Delta S. \tag{10}$$

The difference between month N_1 and N_2 in terms of the mean monthly total TWS anomalies between months N_1 and N_2 is

$$\Delta S_{N_1,N_2} = \overline{S}_{N_2} - \overline{S}_{N_1} = S_0^{N_2} + \frac{1}{D_2}\sum_{N_2,i=1}^{N_2,D_2}(D_2 + 1 - i)\Delta S_{N_2,i} - \left(S_0^{N_1} + \frac{1}{D_1}\sum_{N_1,i=1}^{N_1,D_1}(D_1 + 1 - i)\Delta S_{N_1,i}\right). \tag{11}$$

Substituting Equation (10) into Equation (11), means Equation (11) becomes

$$\Delta S_{N_1,N_2} = \sum_{N_1,i=1}^{N_1,D_1}\Delta S_{N_1,i} + \frac{1}{D_2}\sum_{N_2,i=1}^{N_2,D_2}(D_2 + 1 - i)\Delta S_{N_2,i} - \frac{1}{D_1}\sum_{N_1,i=1}^{N_1,D_1}(D_1 + 1 - i)\Delta S_{N_1,i}. \tag{12}$$

Equation (12) in this study and Equation (4) in Rodell et al. [2] are equivalent to some degree, and they could be converted into each other. Meanwhile, substituting Equation (4) into Equation (12) and taking the ET-related terms as described in Equations (14), Equation (12) can be simplified to:

$$\overline{ET}_{N_1,N_2} = \overline{P}_{N_1,N_2} - \overline{R}_{N_1,N_2} - \Delta S_{N_1,N_2}, \tag{13}$$

$$\overline{ET}_{N_1,N_2} = \sum_{N_1,i=1}^{N_1,D_1}ET_{N_1,i} + \frac{1}{D_2}\sum_{N_2,i=1}^{N_2,D_2}(D_2 + 1 - i)ET_{N_2,i} - \frac{1}{D_1}\sum_{N_1,i=1}^{N_1,D_1}(D_1 + 1 - i)ET_{N_1,i}. \tag{14}$$

The terms $\overline{P}_{N_1,N_2}$ and $\overline{R}_{N_1,N_2}$ can also be expanded as $\overline{ET}_{N_1,N_2}$ in Equation (14). Assuming ET_{N_i} is the total monthly ET for the N_ith month, and using ET_{N_i}/D_i instead of the daily ET for each day in the N_ith month, Equation (14) can be rewritten as:

$$\overline{ET}_{N_1,N_2} = \frac{D_2 + 1}{2D_2}ET_{N_2} + \frac{D_1 - 1}{2D_1}ET_{N_1}. \tag{15}$$

Many studies have estimated the total mean ET in two months ($\overline{ET}$) using Equation (13) [2,8,14]. Considering Equations (13) and (15), the related terms of P and R can be calculated using daily precipitation and runoff observations, as mentioned in Section 3.2, where $\Delta S_{N_1,N_2}$ is the difference in TWS from GRACE in two consecutive months. Here, a set of equations related monthly ET for $N + 1$ months was established, and the observation equation could be written as:

$$\begin{cases} A_{N\times(N+1)}X_{(N+1)\times1} = L_{N\times1} \\ \lambda X_{(N+1)\times1} = I_{(N+1)\times(N+1)} \end{cases} \tag{16}$$

where $N + 1$ is the number of monthly ET to be estimated, and the matrixes $A_{N\times(N+1)}$, $X_{(N+1)\times1}$, $L_{N\times1}$ could be expanded as

$$X_{(N+1)\times1} = [ET_1, ET_2, \cdots ET_{N+1}] \tag{17}$$

$$A(i,j)_{N\times(N+1)} = \begin{cases} \frac{D_{i+1}+1}{2D_{i+1}}, & if\ i = j \\ \frac{D_i-1}{2D_i}, & if\ j = i+1 \\ 0, & else \end{cases}, \text{ where } i = 1, 2, \cdots N, j = 1, 2, \cdots N+1 \tag{18}$$

$$L(i,1)_{N\times1} = \overline{P}_{i,i+1} - \overline{R}_{i,i+1} - \Delta S_{i,i+1}, \text{ where } i = 1, 2, \cdots N \lim_{\delta x \to 0} \tag{19}$$

As for underdetermined system of equations, the constraint equation $\lambda X = I$ was applied to obtain stable solutions, and the appropriate regularization factor λ was determined using the generalized cross validation (GCV) method [44].

The two previous methods and our method were verified by numerical simulation in our study. Firstly, the monthly GRACE-like TWS were calculated from daily *P*, *R*, and ET by using Equation (9). Then, taking the monthly TWS, daily *P* and *R* as observation data, and the ET as the unknown value, we estimated monthly ET using these three methods described above (i.e., Rodell et al. [2], Ramillien et al. [10] and our method). Finally, the monthly ET that converted from the daily ET, which used in the first step to calculating the monthly GRACE-like TWS, was taken as the ET true value (ET0) to verifying these three ET estimations. Including ET_Rodell, the total mean ET in two months based on the method of Rodell et al. [2], ET_Ramillien, the results were obtained from the method of Ramillien et al. [10] and ET_Li, and the method proposed in this study.

In order to analyze the effectiveness of the method and its feasibility in practical applications, the observation error in daily *P* and *R* had to be taken into account. In general, the uncertainties in daily *P* and *R* observations were estimated as 11% and 5%, respectively (Rodell et al. [2,14]). Figure 2 shows ET0 and the ET_Ramillien estimated from GRACE-like TWS and daily *P* and *R* without error and with observation error, using the method introduced by Ramillien et al. [10]. Similarly, Figures 3a and 4a show ET_Li and ET_Rodelll without and with error using the method proposed in this study and Rodell et al. [2]. Furthermore, the regularization factors obtained from the GCV function are also shown in Figures 3b and 4b. The estimation ET_Li and ET_Rodell in Figure 3a are almost completely consistent with ET0, while ET_Ramillien in Figure 2a reflects only the seasonal signal in the ET0 time series, which indicates that the ET estimation method proposed in our study and in Rodell et al. [2] are more credible. The similar results shown in Figure 2a,b reveal that the observation errors of daily *P* and *R* have little influence of the estimation of ET when using the method introduced by Ramillien et al. [10], which both only revealing seasonal signals. The correlation coefficients (R^2) and root mean square error (RMSE) between ET0 and ET estimations were listed in Table 2. The results showed that there is a major improvement for ET_Li relative to ET_Ramillien estimation, while comparing with ET_Rodell, ET_Li estimation has still improved to a certain degree, and the monthly ET value is isolated from ET_Rodell. In conclusion, our method can be used to estimate monthly ET efficiently. The ET results for the case study of the entire YRB discussed below were obtained using our improved approach.
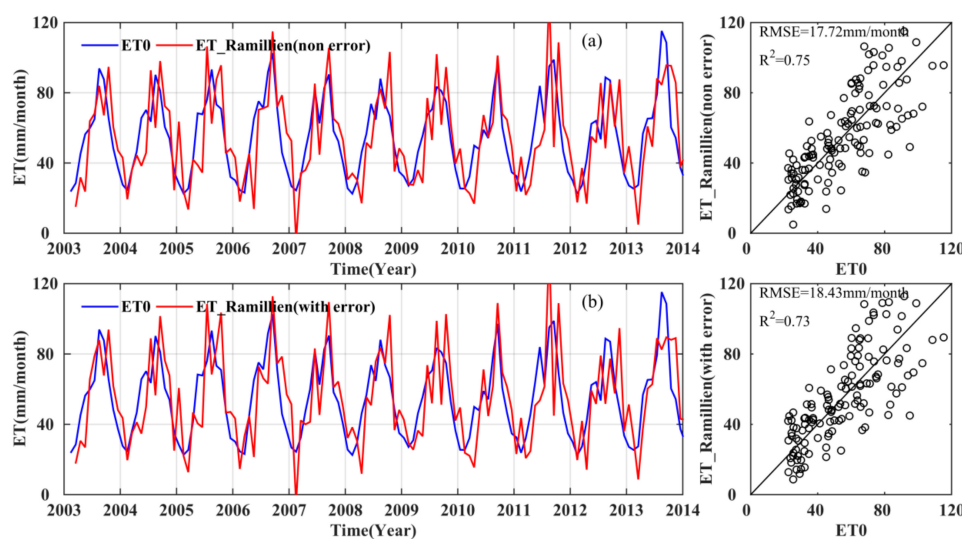

Figure 2. Monthly evapotranspiration (ET) estimated from simulated Gravity Recovery and Climate Experiment (GRACE) terrestrial water storage (TWS) and daily *P* and *R* observations (**a**) without error and (**b**) with error, using the method introduced by Ramillien et al. (2006).
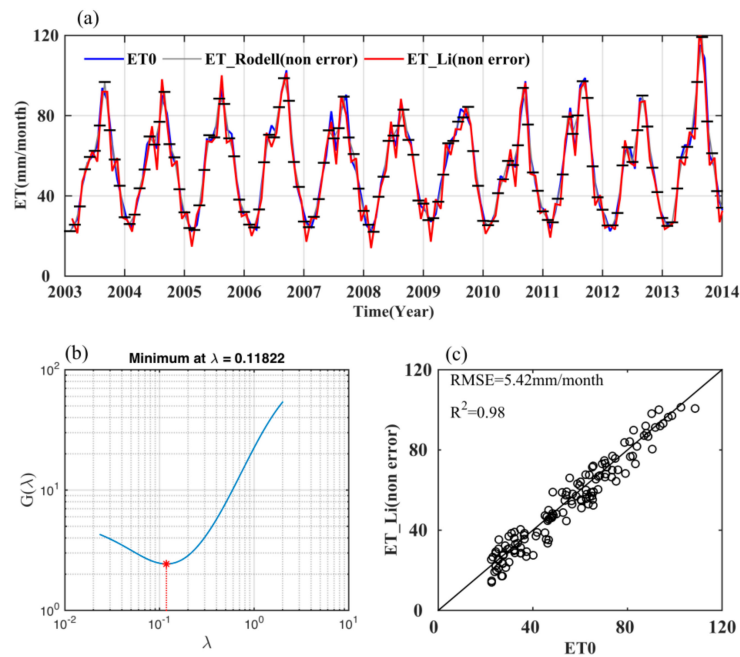
Figure 3. (**a**) Monthly ET estimated from simulated GRACE TWS and daily *P* and *R* observations without error using the method introduced in this study; (**b**) The regularization factor determined by the generalized cross validation (GCV) method; (**c**) The correlation (R^2) and RMSE between the simulated ET observations and ET estimations using our method.
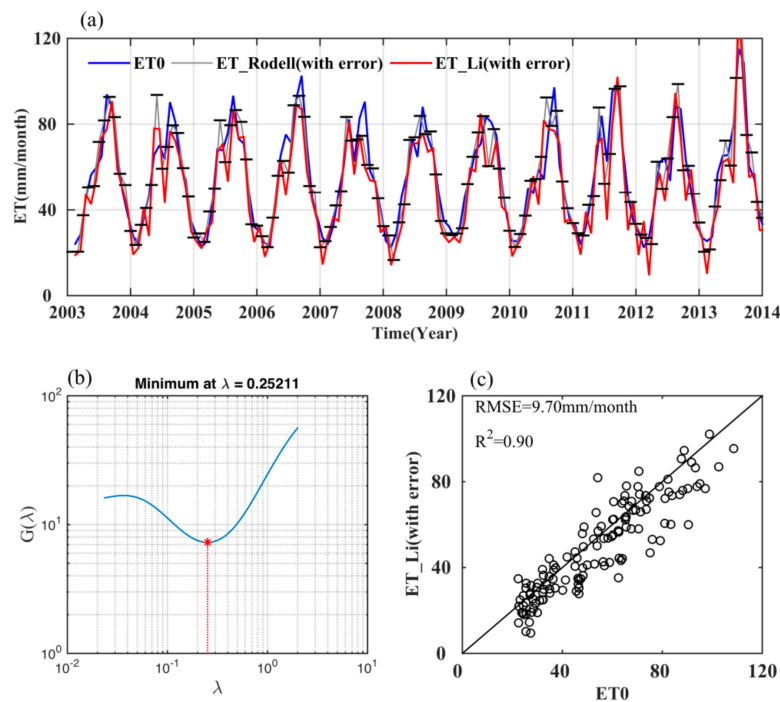
Figure 4. (**a**) Monthly ET estimated from simulated GRACE TWS and daily *P* and *R* observations with error using the method introduced in this study; (**b**) The regularization factor determined by the GCV method; (**c**) The correlation (R^2) and RMSE between the simulated ET observations and ET estimations using our method.

Table 2. The correlation coefficient (R^2) and RMSE between ET0 and ET estimations.

Variable		Non Observation Error			With Observation Error		
		ET_Li	ET_Rodell	ET_Ramillien	ET_Li	ET_Rodell	ET_Ramillien
R^2	ET0	0.98	0.92	0.75	0.90	0.88	0.73
RMSE	ET0	5.42	8.93	17.72	9.70	11.19	18.43

4. Results and Discussion

4.1. ET Estimation Over the YRB

Figure 5a shows the TWSA and TWSC (ΔS) over the entire YRB region from January 2003 to December 2013. The GRACE-derived TWSA contains the mass variations caused by water impoundment in the Three Gorges Reservoir (TGR) [15]. To calculate TWSC deduced from hydrological processes, the mass redistribution caused by water impoundment has to be removed from the GRACE-derived TWSA, and the GRACE-derived TWSC were calculated by Equation (2). Taking the GRACE-derived TWSC and daily *P* and *R* data as inputs, the monthly ET (ET_Li) were estimated using the improved method described in Section 3.3, while the two month mean ET estimation (ET_Rodell) using Rodell et al. [2] were also given (Figure 5b). In addition, the ET from the three products is also shown in Figure 5b,c. The ET_Li and ET from MODIS and GLDAS of the YRB show strongly seasonal signals, reaching maxima around July and August, and minima in January and February. Most of the ET estimations of the YRB show strong seasonality with definite peaks in summer (around June–August) in every year, except for the ET based on in situ observations. The correlation coefficients of ET estimation and ET products were listed in Table 2, and the correlation coefficients between ET_Li and the other six ET time series were all >0.8, which were greater than the correlation coefficients between ET_Rodell and other ET products. The mean annual value of ET_Li is 570 mm/year, and the mean annual values of ET from the other products are all larger than ET_Li to some extent. The mean annual value of ET from MODIS is 676 mm/year, which is slightly larger than ET_Li. The values of ET from the four GLDAS LSMs (CLM, NOAH, VIC, and Mosaic) are 663 mm/year, 836 mm/year, 886 mm/year, and 959 mm/year, respectively. Considering the water balance equation, the ET results should tend to the difference between precipitation and discharge (*P-R* or ET + ΔS) if the mass variation tend to balance (i.e., ΔS tend to zero). The mass variation of the entire YRB observed by GRACE appears to increasing during 2003–2013. The long term trend of the YRB mass variation is 9.07 $\pm$ 3.23 mm/year, which is consistent with the results 8.0 mm/year in Wang et al. [15]. There have been three filling stages of the TGR since May 2003. Since the third filling stage in 2008, the variation of the volume of the TGR has exhibited a seasonal cycle, the amplitude of which becomes stronger as it reaches maximum capacity. Conversely, in response to two severe drought events in the YRB (summer 2006 and spring 2011), the TWSA from GRACE also presents obvious mass decreases during this period. After removing the mass increase attributable to the impounded water of the TGR, the GRACE-derived mass changes tend to balance throughout the estimation period except for slightly decreases in 2006 and 2011. As shown in Table 3, the difference between precipitation and discharge is denoted as ET + ΔS was 570 mm/year. As the mass variations over the entire YRB tend to balance by removing the impact of TGR, the ET provided by three GLDAS models (NOAH, VIC, and Mosaic) appears significantly overestimated.
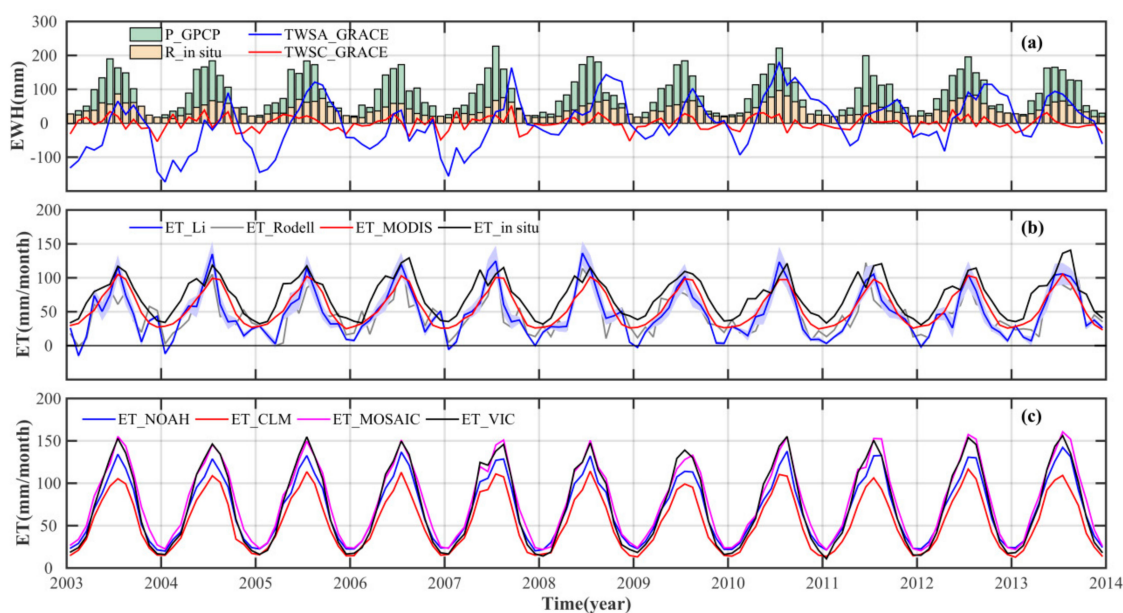
Figure 5. (**a**) Time series of monthly precipitation and runoff from the Datong gauge station, and TWS estimated from GRACE; (**b,c**) ET estimations based on different methods or products over the entire YRB. ET_NOAH, ET_CLM, ET_MOSAIC, and ET_VIC are the ET results obtained from the Global Land Data Assimilation System (GLDAS) products of the four land surface models (LSMs) (Noah, CLM, Mosaic, and VIC), and ET_ MODIS and ET_ in situ are the ET results from Moderate Resolution Imaging Spectroradiometer (MODIS) and in situ observations, respectively.

The monthly values of ET_Li of the seven studied subbasins of the YRB were estimated, and they were evaluated with the ET of the seven subbasins based on the four GLDAS LSMs, MODIS, and in situ data. The correlation coefficients between each two sets revealed that the values of ET_Liwere consistent with the other data, except for those based on in situ observations. The correlation coefficients between ET_Li and ET from the GLDAS CLM over the seven subbasins were all more than 0.69, as showed in Table 4.

Annual ET and auxiliary information relating to the YRB are shown in Table 3. The lowest mean annual *P* and *R* values were obtained in Jinshajiang catchment, which is located in the upstream area of the YRB. There are obvious differences between the areas to the north and south of the main river. The mean annual ET shows a similar pattern in the southern and northern parts of the YRB, consistent with the results in Zhang and Yang (2014). A long-term trend of the YRB mass variation observed by GRACE was caused by water impoundment of the TGR since 2003. While removing the impact of water impoundment, the water shortages over the YRB appear to be accumulating slightly, or tending to being in balance. In other words, the long term trend of ΔS tends to zero, and the ET over the YRB should be tending to ET + ΔS. However, as showed in Table 3, the mean values of annual ET from the four GLDAS models, MODIS, and in situ observations, are all larger than the ET + ΔS value for each basin, which demonstrates that the ET based on these models is overestimated in the YRB.

Each of these datasets was obtained using different observations or methods, leading to differences in the different ET estimations. For instance, the determination of ET based on in situ observations was affected by the sparse and nonuniform distribution of observing stations. Therefore, the reanalysis results cannot reveal complete information for the entire region. Moreover, the empirical formulae or the models and related parameters (i.e., LSMs; LAI (Leaf area index)) used in the estimation of ET from the GLDAS model or MODIS might amplify the differences. As shown in Figure 5c, the ET from the Mosaic model is 50% greater than from the CLM model, which demonstrates that the choice of LSM is crucial in ET estimation. Mu et al. [5] declared that in remotely sensed estimations of ET that consider transpiration from plant surfaces and evaporation from the ground, soil evaporation is the

major component, especially in semiarid and arid systems. LAI models are one of the main ways of distinguishing between vegetation cover and soil. Vinukollu et al. [45] explicitly highlighted that LAI and fractional vegetation cover play important roles in the estimation of ET, especially in humid basins. There are differences between the LAI based on remote sensing and derived from ground measurements attributable to the lack of clumping parameterization, and the magnitude of the error from this source is difficult to estimate.

The inconsistencies in these ET datasets can also be attributed to human activities, i.e., urbanization, intensification of agriculture, and dam construction. Human activities lead to changes in the natural environment through land use change and water management, which not only influence ET, but also complicate the characterization and modeling of the hydrological terms relevant to ET. For instance, in the CSWRB datasets, 428 medium- and large-sized dams were built in the YRB during 2003–2013, adding a total storage capacity of 117.4 km^3, i.e., nearly 13% of the annual discharge. It should be noted that the TGR has the largest dam in the YRB; its completion meant that the storage capacity of the TGR was 4% of the mean annual discharge of the entire basin.

Table 3. Mean values of annual *P*, *R*, ET + Δ*S*, and ET based on different methods for the seven subcatchments and the entire YRB.

| Catchment	P	R	ET + Δ*S*	ET							
				ET_Li	ET_Rodell	CLM	NOAH	Mosaic	VIC	MODIS	In Situ
Jinshajiang	720	301	419	418	420	510	582	681	622	514	907
Wujiang	1029	499	530	529	531	709	892	1019	970	835	635
Minjiang	948	503	445	440	442	656	778	888	746	643	683
Jialingjiang	927	491	436	429	432	683	842	902	854	661	655
Hanjiang	918	439	409	405	408	658	846	916	855	648	694
Dongting Lake	1261	508	822	822	827	749	1006	1166	1098	853	716
Poyang Lake	1507	865	642	643	646	761	1023	1221	1124	859	748
Entire basin (YRB)	1059	488	571	570	571	663	836	959	886	676	733

Table 4. The correlation coefficients (R^2) between ET estimation results (ET_Li and ET_Rodell) and ET from different products.

Catchment	ET_Li						ET_Rodell					
	CLM	NOAH	Mosaic	VIC	MODIS	In Situ	CLM	NOAH	Mosaic	VIC	MODIS	In Situ
Jinshajiang	0.88	0.86	0.87	0.88	0.84	0.36	0.82	0.84	0.84	0.81	0.83	0.25
Wujiang	0.78	0.78	0.76	0.77	0.79	0.72	0.66	0.67	0.67	0.66	0.68	0.66
Minjiang	0.86	0.88	0.86	0.87	0.87	0.75	0.78	0.80	0.79	0.78	0.80	0.64
Jialingjiang	0.71	0.76	0.71	0.72	0.71	0.79	0.74	0.75	0.72	0.72	0.72	0.70
Hanjiang	0.78	0.71	0.65	0.71	0.68	0.55	0.74	0.69	0.64	0.70	0.68	0.58
Dongting Lake	0.69	0.71	0.66	0.67	0.66	0.71	0.71	0.69	0.67	0.68	0.70	0.65
Poyang Lake	0.71	0.65	0.60	0.67	0.64	0.57	0.68	0.63	0.60	0.65	0.66	0.58
Entire basin (YRB)	0.88	0.88	0.86	0.87	0.87	0.83	0.82	0.83	0.82	0.82	0.85	0.78

4.2. Comparing ET Anomalies with P and TWS Anomalies

Figure 6 presents the non-seasonal TWS anomalies from GRACE over the seven subbasins smoothed by a 13-month moving average filter, coupled with the non-seasonal ET and *P* anomalies from 2003 to 2013. The TWS anomaly is negative during drought events, e.g., summer 2006 in upper reaches of YRB, spring 2011 in the south YRB (i.e., Wujiang, Dongting Lake and Poyang Lake). The upper reaches of the YRB had 19~38% less rainfall and 3~19% more evapotranspiration in summer 2006 than in an average year. There was also less rainfall during fall 2009 to spring 2010 drought (9~22%) and spring 2011 drought (20~29%), but no continuous and efficient positive ET during these drought events. It is clear that precipitation has extremely low values in each drought; however, evapotranspiration only appears obviously high during the 2006 summer drought in the upper basin.

The YRB is located in the region of the Asian monsoon, which is influenced by the El Nino/Southern Oscillation (ENSO) via the strength of the subtropical high in the western Pacific region. Earlier studies have suggested that ENSO shows a close relation with flood and drought events in the YRB region [46,47]. The droughts in 2006 and 2009–2010 clearly correspond to El Nino events (+0.5 °C SST in the tropical Pacific). Accompanying the formation of the El Nino from May 2006, the amplification of both the western Pacific subtropical high and the Tibetan high contributed to the formation of a unified subtropical belt of high pressure that blocked water vapor transport, resulting in lower levels of precipitation than normal, especially in Sichuan and Chongqing provinces from June to August [48]. In addition, this subtropical belt of high pressure also resulted in warmer surface temperatures at the same time [49]. Similarly, in September 2009, an El Nino event occurred that resulted in an anomalous anticyclonic flow field in the South China Sea and the western Pacific. This caused the position of the western Pacific subtropical high to shift further southwestward than normal. Consequently, in conjunction with a descending flow anomaly behind the trough controlled by the eastern part of the Tibetan Plateau, water vapor was blocked from being transported from the Bay of Bengal toward the Yunnan–Guizhou Plateau [50,51]. This resulted in a prolonged period of reduced rainfall and warmer temperatures in this region. Furthermore, responding to a negative phase of the Arctic Oscillation, the East Asian winter monsoon was stronger and further eastward, which led to weakening of the cold air arriving over Southwest China and less precipitation in the following drought [52]. Differently, during the 2011 drought, the ENSO was in the La Nina phase, yet the sea surface Temperature of the South Indian Ocean maintained a persistent positive anomaly [53]. The abnormality of SST made the western Pacific subtropical high weaker than normal and it retreated eastward, suppressing the transport of water vapor to the middle and lower regions of the YRB. Meanwhile, because of the stronger-than-normal meridional circulation and the corresponding northerly wind, the air over the middle and lower YRB was drier, but colder than normal [54]. The abnormal climate we discussed above was good enough to explain the less rainfall during drought events. However, the factors of ET variety were still ambiguous, and the relationship between the meteorological factor and hydrological factor needs to be further discussed.
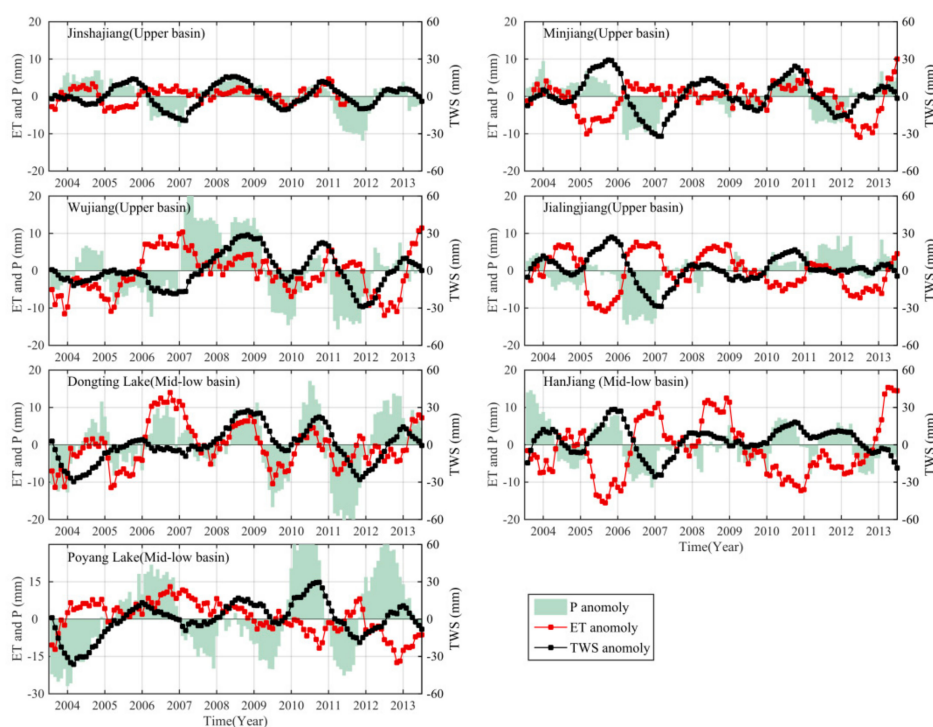
Figure 6. The non-seasonal TWS anomaly from GRACE, ET from the water balance method, and precipitation from the Global Precipitation Climatology Project (GPCP) dataset 2003–2013, smoothed using the 13-month moving average filter.

4.3. Limiting Factors of ET

As one of the most important components in the climate system and terrestrial water cycle, ET is affected by the interaction between climate change and soil moisture variation. There is debate in the field of ecological hydrology over whether ET response is due primarily to atmospheric demand or to terrestrial moisture-supply limitation [55]. Intuitively, it could be considered that ET would respond to atmospheric changes when the moisture supply is sufficient. Conversely, ET could be restricted by soil moisture supply when the soil is too dry. Syed et al. [11] inferred that ET over the Ganga River Basin is limited primarily by soil moisture supply, whereas Karam and Bras [56] suggested that Amazonian ET is predominantly limited by energy availability. Many meteorological parameters affect ET, including ground surface temperature (TEM), sunshine duration, relative humidity (RHU), wind speed (WIN), and vapor pressure deficit, all of which are correlated strongly with near-surface temperature. Therefore, temperature has often been used as a proxy for atmospheric demand in previous research on the correlation between ET and atmospheric demand. Here, in order to distinguish the primary limitation of ET over the YRB, we analyzed independent estimations of TEM, RHU, WIN, and soil moisture (SM) over the study region.

The meteorological data, including TEM, RHU, and WIN used here, were provided by the CGCD, and the monthly TEM, RHU, and WIN data averaged over the YRB region were acquired by resampling of daily observations using the same processing method mentioned above. Time series of soil moisture data, averaged over the YRB region, were derived using the $0.5° \times 0.5°$ gridded monthly global soil moisture datasets produced by the Climate Prediction Center [57]. Figure 7a shows the temporal variations of ET and temperature averaged over the entire YRB, which were smoothed using a 13-month moving average filter. The two time series are coherent, with a correlation coefficient of 0.69. Both reveal a slight trend of increase from 2003 to 2007, albeit with a lower value in 2005, but appear balanced in the other years. As shown in Figure 7b–d, there is no strong correlation between the time series of ET and RHU, WIN, and SM. However, it should be noted that there were lower RHU and higher

WIN during drought events in summer 2006, from autumn 2009 to spring 2011 and in spring 2011, while higher temperatures were obvious only during 2006. Table 5 presents the correlation coefficients between each hydrological component. The results reveal that soil moisture is closely related to the combined effect of precipitation and ET, i.e., it is responsive to inputs and outputs of water. Based on the above results, we can infer that ET changes in the YRB region are caused by variation in atmospheric demand. This conclusion is in accord with Jung et al. [55], who demonstrated that atmospheric demand (i.e., temperature) in China is the primary factor limiting the change of ET, because the trends of change of ET and soil moisture are opposed [55] (see [55] Figure 2).
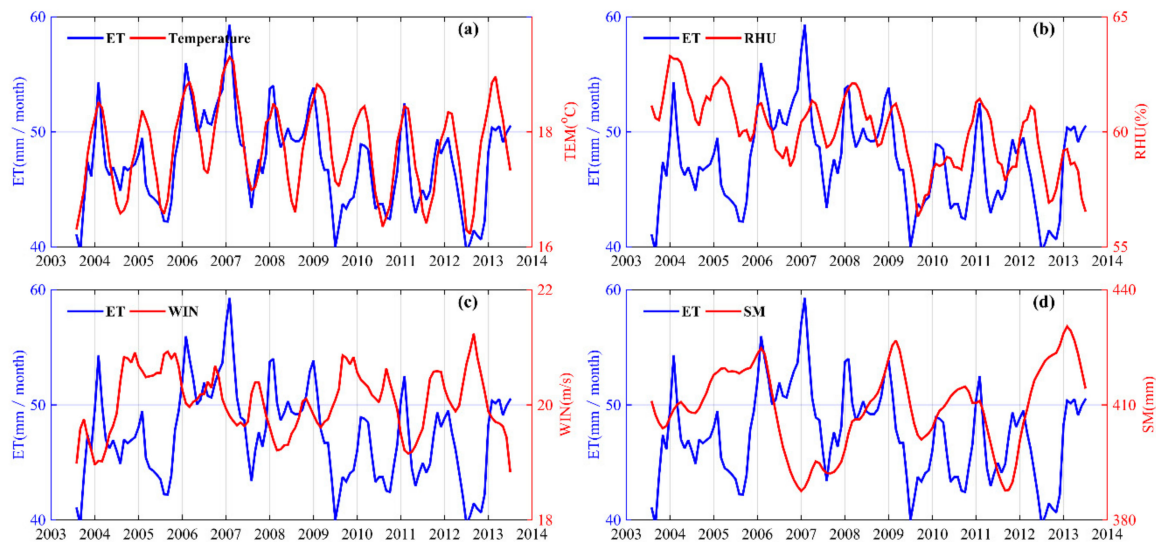
Figure 7. Time series smoothed using 13-month moving average filter: (**a**) ET and temperature (TEM), (**b**) ET and relative humidity (RHU), (**c**) ET and wind speed (WIN) and (**d**) ET and soil moisture (SM).

Table 5. Correlation coefficient between each hydrological component, based on the time series smoothed using the 13-month moving average filter, as in Figure 7.

Variable	*P*	*R*	ET	*SM*	*P*-ET
P	1.00	0.71	0.34	0.47	0.79
R	0.71	1.00	−0.29	0.77	0.90
ET	0.34	−0.29	1.00	−0.17	−0.31
SM	0.47	0.77	−0.17	1.00	0.59
P-ET	0.79	0.90	−0.31	0.59	1.00

We also calculated the mean annual *P* and ET over the seven subcatchments, together with the mean annual values of TEM, RHU, and WIN, as shown in Figure 8. The seven subcatchments were divided into three regions according to the geographical features mentioned in Section 4.1. Region 1 comprises just the Jinshajiang subcatchments; Region 2 covers the northern YRB, i.e., the Minjiang, Jialingjiang, and Hanjiang subcatchments; and Region 3 includes the Wujiang, Dongting Lake, and Poyang Lake subcatchments in the southern YRB. Overall, the mean annual ET in the southern YRB is larger than in the northern YRB, which is consistent with temperature, i.e., the mean annual temperature in the south is higher than in the north. Figure 8 reveals that the mean annual ET in the Jinshajiang basin is the same as in the northern YRB, despite it having less precipitation and lower temperatures. This is because the lower relative humidity and higher wind speed benefits ET. There are no significant differences in the mean annual values of ET in Region 2. Each subcatchment in this region has its own particular conditions that affect ET, e.g., Minjiang with low relative humidity, Jialingjiang with high temperature, and HJ with high wind speed. Given

the ample precipitation and high temperatures in the southern YRB, the mean annual ET reaches a maximum in Region 3. In the southern YRB, the mean annual temperature increases from east to west, but the mean annual ET of Dongting Lake is higher than that of Wujiang and Poyang Lake because of its lower relative humidity and higher wind speed. It could be inferred that in addition to temperature, both relative humidity and wind speed represent factors that limit the spatial distribution of ET variation. The spatial distribution of mean annual ET estimated using our proposed method is consistent with the distributions of the limitation factors.
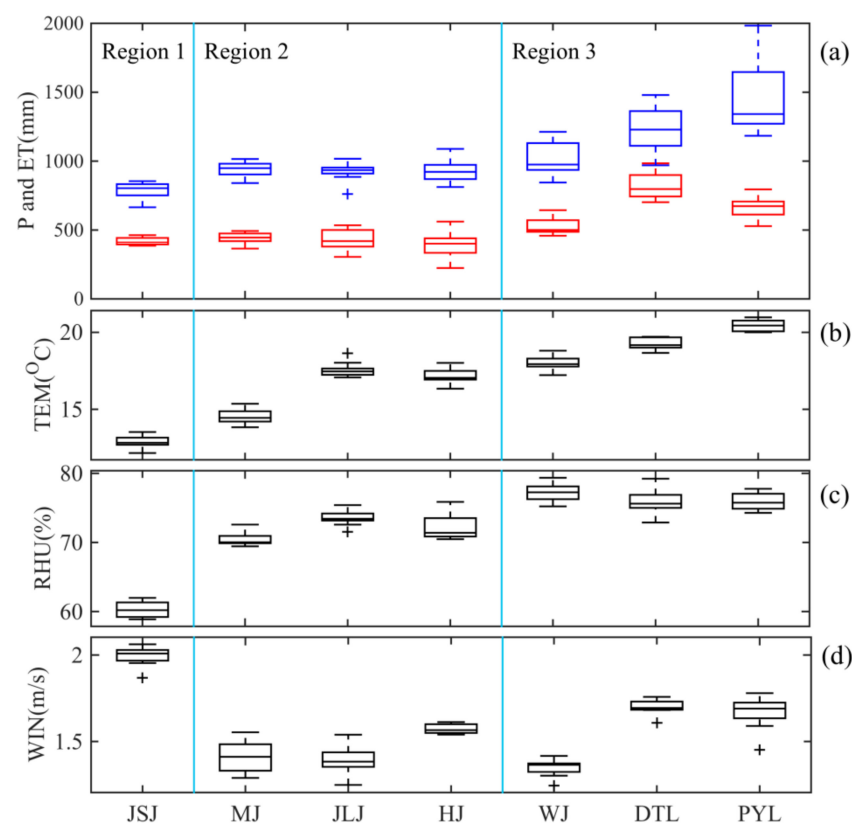
Figure 8. Limitation factors of ET in the seven subcatchments, i.e., TEM, RHU, and WIN. And the name for each subcatchment are Jinshajiang (JSJ), Minjiang(MJ), Jialinjiang (JLJ), Hanjiang (HJ), Wujiang (WJ), Dongting Lake (DTL), and Poyang Lake (PYL). For each box, the central mark is the median, edges represent the 25th and 75th percentiles, and whiskers extend to the furthest data points not considered outliers (outliers are plotted individually). (**a**) Blue boxes denote precipitation (*P*) for each region, and red boxes denote ET for each subcatchment; Boxes in (**b–d**) denote temperature (TEM), relative humidity (RHU), and wind speed (WIN) for each subcatchment, respectively.

5. Conclusions

The results of this study showed that the improved method proposed here is valid and viable. Comparing monthly ET estimations from our method with results obtained from previous methods by simulation, the simulation results revealed that the ET estimation method could isolate the monthly signal from the GRACE monthly gravity field models and the daily precipitation and discharge data. Considering the YRB as an example, the spatially averaged values of ET of the YRB and of its seven subcatchments were estimated using our proposed method for the period 2003–2013.Comparison of the values of ET_Li with different ET products showed good overall agreement, especially on the seasonal timescale. The mean values of ET_Li were close to the ET estimates derived from the GLDAS CLM and the MODIS model, whereas the ET derived from the other three GLDAS models (NOAH, VIC, and Mosaic) appeared overestimated when considering the water mass balance of the YRB region.

The method proposed in this study was proven applicable for estimating ET. The level of consistency between the ET from GRACE and other ET products demonstrated that GRACE observations could be used to analyze and predict ET on a regional scale, such as the YRB.

We also analyzed the correlation between ET and independent estimations of meteorological factors and soil moisture. Spatially averaged ET was found distinctly more coherent with near-surface temperature (R^2 = 0.69) than with other factors, which suggests that atmospheric demand is the dominant factor controlling ET variability in the YRB. The relationship between the mean annual ET of the seven subcatchments and atmospheric conditions were analyzed, which showed that the spatial distribution of the mean annual ET obtained using our method was consistent with atmospheric conditions. These results are considered to have improved the understanding of the role of ET in hydrological cycle of the study region.

Conjunct with daily P and R data, more details of monthly ET were isolated from monthly gravity field models from GRACE, which indicated that multiresolution datasets fusion were more effective for extracting information from hydrological components. The continuation of GRACE by its follow up, GRACE Follow On mission, will provide the continuous data as GRACE with higher temporal–spatial resolution. Furthermore, based on these observation data, our methodology could be applied to assess ET variation with a shorter time interval (i.e., weekly or ten days), which will useful for better understanding of hydrologic processes especially in basins with complex environment.

Author Contributions: Q.L., Z.L. and B.Z. designed the research; Q.L. and H.Z. conducted the experiments and analyzed the data. All authors contributed to writing the manuscript; Q.L. and Z.L. revised the manuscript.

Conflicts of Interest: The authors declare no conflict of interest.

Abbreviations

TWSA	terrestrial water storage anomalies
TWSC/ΔS	terrestrial water storage change
SM	soil moisture
TEM	near-surface temperature
RHU	relative humidity
WIN	wind speed

References

1. Moiwo, J.P.; Tao, F. Satellite signal shows storage-unloading subsidence in North China. *Hydrol. Earth Syst. Sci. Discuss.* **2015**, *12*, 6043–6075. [CrossRef]
2. Rodell, M.; Famiglietti, J.S.; Chen, J.; Seneviratne, S.I.; Viterbo, P.; Holl, S.; Wilson, C.R. Basin scale estimates of evapotranspiration using GRACE and other observations. *Geophys. Res. Lett.* **2004**, *31*, L20504. [CrossRef]
3. Billah, M.M.; Goodall, J.L.; Narayan, U.; Reager, J.T.; Lakshmi, V.; Famiglietti, J.S. A methodology for evaluating evapotranspiration estimates at the watershed-scale using GRACE. *J. Hydrol.* **2015**, *523*, 574–586. [CrossRef]
4. Long, D.; Longuevergne, L.; Scanlon, B.R. Uncertainty in evapotranspiration from land surface modeling, remote sensing, and GRACE satellites. *Water Resour. Res.* **2014**, *50*, 1131–1151. [CrossRef]
5. Mu, Q.; Heinsch, F.A.; Zhao, M.; Running, S.W. Development of a global evapotranspiration algorithm based on MODIS and global meteorology data. *Remote Sens. Environ.* **2007**, *111*, 519–536. [CrossRef]

6. Fisher, J.B.; Tu, K.P.; Baldocchi, D.D. Global estimates of the land–atmosphere water flux based on monthly AVHRR and ISLSCP-II data, validated at 16 FLUXNET sites. *Remote Sens. Environ.* **2008**, *112*, 901–919. [CrossRef]

7. Rodell, M.; Houser, P.R.; Jambor, U.; Gottschalck, J.; Mitchell, K.; Meng, C.J.; Arsenault, K.; Cosgrove, B.; Radakovich, J.; Bosilovich, M.; et al. The global land data assimilation system. *Bull. Am. Meteorol. Soc.* **2004**, *85*, 381–394. [CrossRef]

8. Castle, S.L.; Reager, J.T.; Thomas, B.F.; Purdy, A.J.; Lo, M.-H.; Famiglietti, J.S.; Tang, Q. Remote detection of water management impacts on evapotranspiration in the Colorado River basin. *Geophys. Res. Lett.* **2016**, *43*, 5089–5097. [CrossRef]

9. Cesanelli, A.; Guarracino, L. Estimation of regional evapotranspiration in the extended Salado Basin (Argentina) from satellite gravity measurements. *Hydrogeol. J.* **2011**, *19*, 629–639. [CrossRef]

10. Ramillien, G.; Frappart, F.; Güntner, A.; Ngo-Duc, T.; Cazenave, A.; Laval, K. Time variations of the regional evapotranspiration rate from Gravity Recovery and Climate Experiment (GRACE) satellite gravimetry. *Water Resour. Res.* **2006**, *42*. [CrossRef]

11. Syed, T.H.; Webster, P.J.; Famiglietti, J.S. Assessing variability of evapotranspiration over the ganga river basin using water balance computations. *Water Resour. Res.* **2014**, *50*, 2551–2565. [CrossRef]

12. Zeng, Z.; Wang, T.; Zhou, F.; Ciais, P.; Mao, J.; Shi, X.; Piao, S. A worldwide analysis of spatiotemporal changes in water balance-based evapotranspiration from 1982 to 2009. *J. Geophys. Res. Atmos.* **2014**, *119*, 1186–1202. [CrossRef]

13. Pan, Y.; Zhang, C.; Gong, H.; Yeh, P.J.F.; Shen, Y.; Guo, Y.; Huang, Z.; Li, X. Detection of human-induced evapotranspiration using GRACE satellite observations in the Haihe River basin of China. *Geophys. Res. Lett.* **2017**, *44*, 190–199. [CrossRef]

14. Rodell, M.; McWilliams, E.B.; Famiglietti, J.S.; Beaudoing, H.K.; Nigro, J. Estimating evapotranspiration using an observation based terrestrial water budget. *Hydrol. Processes* **2011**, *25*, 4082–4092. [CrossRef]

15. Wang, X.; de Linage, C.; Famiglietti, J.; Zender, C.S. Gravity recovery and climate experiment (GRACE) detection of water storage changes in the three gorges reservoir of China and comparison with in situ measurements. *Water Resour. Res.* **2011**, *47*, W12502. [CrossRef]

16. Han, S.-C. Improved estimation of terrestrial water storage changes from GRACE. *Geophys. Res. Lett.* **2005**, *32*. [CrossRef]

17. Tapley, B.D.; Bettadpur, S.; Ries, J.C.; Thompson, P.F.; Watkins, M.M. Grace measurements of mass variability in the earth system. *Science* **2004**, *305*, 503–505. [CrossRef] [PubMed]

18. Cazenave, A.; Chen, J. Time-variable gravity from space and present-day mass redistribution in the Earth system. *Earth Planet. Sci. Lett.* **2010**, *298*, 263–274. [CrossRef]

19. Syed, T.H.; Famiglietti, J.S.; Rodell, M.; Chen, J.; Wilson, C.R. Analysis of terrestrial water storage changes from GRACE and GLDAS. *Water Resour. Res.* **2008**, *44*. [CrossRef]

20. Wahr, J. Time-variable gravity from GRACE: First results. *Geophys. Res. Lett.* **2004**, *31*. [CrossRef]

21. Jacob, T.; Wahr, J.; Pfeffer, W.T.; Swenson, S. Recent contributions of glaciers and ice caps to sea level rise. *Nature* **2012**, *482*, 514–518. [CrossRef] [PubMed]

22. Velicogna, I. Short term mass variability in Greenland, from GRACE. *Geophys. Res. Lett.* **2005**, *32*. [CrossRef]

23. Cazenave, A.; Dominh, K.; Guinehut, S.; Berthier, E.; Llovel, W.; Ramillien, G.; Ablain, M.; Larnicol, G. Sea level budget over 2003–2008: A reevaluation from GRACE space gravimetry, satellite altimetry and Argo. *Glob. Planet. Chang.* **2009**, *65*, 83–88. [CrossRef]

24. Chen, J.L.; Wilson, C.R.; Tapley, B.D.; Famiglietti, J.S.; Rodell, M. Seasonal global mean sea level change from satellite altimeter, GRACE, and geophysical models. *J. Geodesy* **2005**, *79*, 532–539. [CrossRef]

25. Han, S.-C.; Sauber, J.; Luthcke, S. Regional gravity decrease after the 2010 Maule (Chile) earthquake indicates large-scale mass redistribution. *Geophys. Res. Lett.* **2010**, *37*. [CrossRef]

26. Han, S.C.; Shum, C.K.; Bevis, M.; Ji, C.; Kuo, C.Y. Crustal dilatation observed by GRACE after the 2004 Sumatra-Andaman earthquake. *Science* **2006**, *313*, 658–662. [CrossRef] [PubMed]

27. Matsuo, K.; Heki, K. Coseismic gravity changes of the 2011 Tohoku-Oki earthquake from satellite gravimetry. *Geophys. Res. Lett.* **2011**, *38*, L00G12. [CrossRef]

28. Abelen, S.; Seitz, F.; Abarca-del-Rio, R.; Güntner, A. Droughts and floods in the la plata basin in soil moisture data and GRACE. *Remote Sens.* **2015**, *7*, 7324–749. [CrossRef]

29. Chen, J.L.; Wilson, C.R.; Tapley, B.D.; Yang, Z.L.; Niu, G.Y. 2005 drought event in the Amazon River basin as measured by GRACE and estimated by climate models. *J. Geophys. Res.* **2009**, *114*. [CrossRef]

30. Zhou, H.; Luo, Z.; Tangdamrongsub, N.; Wang, L.; He, L.; Xu, C.; Li, Q. Characterizing drought and flood events over the Yangtze River basin using the HUST-GRACE2016 solution and ancillary data. *Remote Sens.* **2017**, *9*, 1100. [CrossRef]

31. Rodell, M.; Velicogna, I.; Famiglietti, J.S. Satellite-based estimates of groundwater depletion in India. *Nature* **2009**, *460*, 999–1002. [CrossRef] [PubMed]

32. Feng, W.; Zhong, M.; Lemoine, J.-M.; Biancale, R.; Hsu, H.-T.; Xia, J. Evaluation of groundwater depletion in North China using the gravity recovery and climate experiment (GRACE) data and ground-based measurements. *Water Resour. Res.* **2013**, *49*, 2110–2118. [CrossRef]

33. Chen, J.L.; Wilson, C.R.; Tapley, B.D.; Scanlon, B.; Güntner, A. Long-term groundwater storage change in Victoria, Australia from satellite gravity and in situ observations. *Glob. Planet. Chang.* **2016**, *139*, 56–65. [CrossRef]

34. Eicker, A.; Schumacher, M.; Kusche, J.; Döll, P.; Schmied, H. Calibration/data assimilation approach for integrating GRACE data into the WaterGAP Global Hydrology Model (WGHM) using an ensemble Kalman Filter: First results. *Surv. Geophys.* **2014**, *35*, 1285–1309. [CrossRef]

35. Güntner, A. Improvement of global hydrological models using GRACE data. *Surv. Geophys.* **2008**, *29*, 375–397. [CrossRef]

36. Li, B.; Rodell, M.; Zaitchik, B.F.; Reichle, R.H.; Koster, R.D.; van Dam, T.M. Assimilation of GRACE terrestrial water storage into a land surface model: Evaluation and potential value for drought monitoring in western and central Europe. *J. Hydrol.* **2012**, *446–447*, 103–115. [CrossRef]

37. Niu, G.-Y.; Yang, Z.-L. Assessing a land surface model's improvements with GRACE estimates. *Geophys. Res. Lett.* **2006**, *33*. [CrossRef]

38. Chen, J.; Wu, X.; Finlayson, B.L.; Webber, M.; Wei, T.; Li, M.; Chen, Z. Variability and trend in the hydrology of the Yangtze River, China: Annual precipitation and runoff. *J. Hydrol.* **2014**, *513*, 403–412. [CrossRef]

39. Hao, Z.C.; Yang, R.R.; Chen, X.M.; Chen, X.; Liang, Z.H.; Dawa, D.Z. Tempo-spatial patterns of the potential evaporation in the Yangtze River Catchment for the period 1960–2011. *J. Glaciol. Geocryol.* **2013**, *35*, 408–419.

40. Zhang, Z.-Z.; Chao, B.F.; Lu, Y.; Hsu, H.-T. An effective filtering for GRACE time-variable gravity: Fan filter. *Geophys. Res. Lett.* **2009**, *36*, L17311. [CrossRef]

41. Swenson, S.; Wahr, J. Post-processing removal of correlated errors in GRACE data. *Geophys. Res. Lett.* **2006**, *33*. [CrossRef]

42. Chen, J.L. Low degree spherical harmonic influences on gravity recovery and climate experiment (GRACE) water storage estimates. *Geophys. Res. Lett.* **2005**, *32*. [CrossRef]

43. Huffman, G.J.; Adler, R.F.; Arkin, P.; Chang, A.; Ferraro, R.; Gruber, A.; Janowiak, J.; McNab, A.; Rudolf, B.; Schneider, U. The global precipitation climatology project (GPCP) combined precipitation dataset. *Bull. Am. Meteorol. Soc.* **1997**, *78*, 5–20. [CrossRef]

44. Golub, G.H.; Heath, M.; Wahba, G. Generalized cross-validation as a method for choosing a good ridge parameter. *Technometrics* **1979**, *21*, 215–223. [CrossRef]

45. Vinukollu, R.K.; Meynadier, R.; Sheffield, J.; Wood, E.F. Multi-model, multi-sensor estimates of global evapotranspiration: Climatology, uncertainties and trends. *Hydrol. Processes* **2011**, *25*, 3993–4010. [CrossRef]

46. Xiao, M.; Zhang, Q.; Singh, V.P. Influences of ENSO, NAO, IOD and PDO on seasonal precipitation regimes in the Yangtze River basin, China. *Int. J. Climatol.* **2014**, *35*, 3556–3567. [CrossRef]

47. Zhang, Z.; Chao, B.F.; Chen, J.; Wilson, C.R. Terrestrial water storage anomalies of Yangtze River basin droughts observed by GRACE and connections with ENSO. *Glob. Planet. Chang.* **2015**, *126*, 35–45. [CrossRef]

48. Xu, J.J.; He., Q.; Liu, H.; Chen, J.Y. Preliminary analysis of characteristics of the exceptional low discharge and IST cause over the Yangtze River, 2006. *Resour. Environ. Yangtze Basin* **2008**, 716–722.

49. Peng, J.B.; Zhang, Q.Y.; Bueh, C. On the Characteristics and possible cause of a serve drought and heat wave in the Sichuan-Chongqing region in 2006. *Clim. Environ. Res.* **2007**, *12*, 464–474. (In Chinese)

50. Duan, H.X.; Wang, J.; Liu, Y.; Li, Y.; Wang, S. The features of continuous heavy drought from autumn 2009 to spring 2010 in southwest China and analysis of its atmospheric circulation anomalies. *J. Glaciol. Geocryol.* **2013**, *35*, 1022–1035.

51. Huang, R.; Liu, Y.; Wang, L.; Wang, L. Analysis of the causes of severe drought occurring in Southwest China from the fall of 2009 to the spring of 2010. *Chin. J. Atmos. Sci.* **2012**, *36*, 443–457.

52. Lu, E.; Luo, Y.; Zhang, R.; Wu, Q.; Liu, L. Regional atmospheric anomalies responsible for the 2009–2010 severe drought in China. *J. Geophys. Res. Atmos.* **2011**, *116*. [CrossRef]

53. Tang, J.; Cheng, H.; Liu, L. Assessing the recent droughts in southwestern china using satellite gravimetry. *Water Resour. Res.* **2014**, *50*, 3030–3038. [CrossRef]

54. Lu, E.; Liu, S.; Luo, Y.; Zhao, W.; Li, H.; Chen, H.; Zeng, Y.; Liu, P.; Wang, X.; Higgins, R.W.; et al. The atmospheric anomalies associated with the drought over the Yangtze River basin during spring 2011. *J. Geophys. Res. Atmos.* **2014**, *119*, 5881–5894. [CrossRef]

55. Jung, M.; Reichstein, M.; Ciais, P.; Seneviratne, S.I.; Sheffield, J.; Goulden, M.L.; Bonan, G.; Cescatti, A.; Chen, J.; de Jeu, R.; et al. Recent decline in the global land evapotranspiration trend due to limited moisture supply. *Nature* **2010**, *467*, 951–954. [CrossRef] [PubMed]

56. Karam, H.N.; Bras, R.L. Climatological basin-scale Amazonian evapotranspiration estimated through a water budget analysis. *J. Hydrometeorol.* **2008**, *9*, 1048–1060. [CrossRef]

57. Fan, Y.; van den Dool, H. Climate prediction center global monthly soil moisture data set at 0.5° resolution for 1948 to present. *J. Geophys. Res. Atmos.* **2004**, *109*. [CrossRef]